Chapter 3
Acceleration Effect

Dale P. Barkey

3.1 Introduction

Fabrication of microscale and nanoscale structures can be implemented by electrodeposition of copper onto conductive templates that contain recesses in form of the desired structure. The current distribution that results from deposition from a simple acid copper solution is concentrated near the upper corners of recesses and results in incomplete filling, formation of voids, and a substantial overburden of nonfunctional material. In industrial practice, effective filling of features such as trenches and vias by copper electrodeposition relies on additive ensembles that promote bottom-up filling, uniform current macrodistribution and minimal overburden.

The components of these additive systems include suppressors, accelerants, and levelers. Suppressors and levelers both inhibit electrodeposition. For our purposes, a suppressor is an inhibitor that can be deactivated by an accelerant. Suppressors include polyalkyl glycols (PAG) such as polyethylene glycol (PEG). They are weakly adsorbed on the surface in combination with chloride and are not consumed or chemically transformed on the metal surface. Levelers, such as Janus Green B, are inhibitors that are not deactivated by accelerants. They are strongly adsorbed and are consumed on the metal surface. Filling of microscale and nanoscale features is achieved through one of two broad categories of mechanism [1]. One of these is the diffusion-limited consumption of leveler. This mechanism has been understood for decades and is the basis for leveling on many different physical scales. Since it does not involve an accelerant, it will not be considered further. The other mechanism relies on the combination of suppressor and accelerant. In this latter type of mechanism, the accelerant is concentrated at the bottom of features and deactivates or excludes the suppressor there. Accelerants have been postulated to lift or displace adsorbed suppressors from the surface and restore the

D. P. Barkey (✉)
Department of Chemical Engineering, College of Engineering and Physical Science, Kingsbury Hall, Room W305, Durham, NH 03824, USA
e-mail: dpb@cisunix.unh.edu

K. Kondo et al. (eds.), *Copper Electrodeposition for Nanofabrication of Electronics Devices*, Nanostructure Science and Technology 171, DOI: 10.1007/978-1-4614-9176-7_3,

higher rate of deposition observed on the suppressor-free surface. While the application considered here is the filling of trenches, vias, or other substrate features that act as templates for fabrication of microscale and nanoscale structures, the principle is the same as that which produces bright deposits in more conventional plating, and the accelerant is sometimes referred to as a brightener.

While many suppressors and levelers can be found in the literature, few effective accelerants are known. In the open literature, most reports concern bis(3-sulfopropyl) disulfide (SPS) or its reduced monomer, 3-mercaptopropylsulfonate (MPS) (see, Fig. 3.1). The solution and surface chemistries of this compound in acid-sulfate copper-plating solutions are more complicated than those of either suppressors or levelers. Both the sulfate functional group and the sulfur–sulfur bond (in SPS) or thiolate (formed by MPS) appear to play critical roles in the accelerant mechanism. In contrast to suppressors, these molecules are consumed at a high rate in plating operations, and the rate of consumption is sensitive to the cell configuration and applied current waveform.

What follows is a review of chemical and electrochemical studies of these accelerant compounds as well as mechanistic models of their role in filling processes. We begin with a consideration of the homogeneous solution chemistry of SPS and MPS and their interactions with other components of the bath. These interactions include transformations of the molecules into the effective accelerant as well as their degradation and deactivation. We then turn to their adsorption on copper and to the effect of applied potential on their surface chemistry. Finally, we consider the models that have been proposed to describe the role played by accelerants in the filling of features on various spatial and temporal scales.

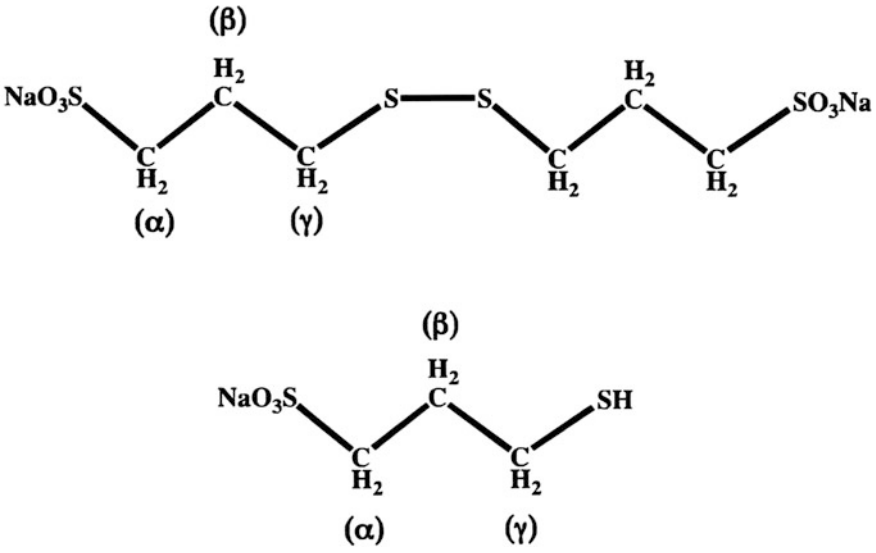

Fig. 3.1 The SPS and MPS molecules, shown here as sodium salts. Reproduced with permission from Garcia-Cardona et al. [9], their Fig. 3.1

3.2 Solution Chemistry

SPS and MPS are added in parts per million (ppm) concentrations to acid-sulfate copper plating baths. These baths also contain chloride in concentrations in the tens of ppm range. Chloride is known to play a role in both copper deposition and in the function of the accelerant. There is considerable evidence that Cu(I) interacts with SPS and MPS as well. An important feature of acid-sulfate copper plating baths is the fact that the reduction potential of Cu(I) is substantially positive of the reduction potential of Cu(II), the main form of copper in solution. In equilibrium with the metal, the concentration of Cu(I) is therefore much lower than the concentration of Cu(II). Moreover, in practical plating operations, the metal and solution are not in equilibrium at open circuit. Dissolved oxygen oxidizes Cu(I) to Cu(II), so that the bulk aerated solution contains a concentration of Cu(I) that is lower than the equilibrium value. Under this condition, the metal corrodes by proportionation,

$$\mathrm{Cu(II)} + \mathrm{Cu} = 2\mathrm{Cu(I)} \tag{3.1}$$

and Cu(I) is generated at the metal-solution interface. Chloride, on the other hand, stabilizes Cu(I) through formation of CuCl and $CuCl_2^-$. For these reasons, the interactions in solution among SPS, MPS, Cu(I), chloride, and oxygen are of interest.

The role of chloride in accelerant function was demonstrated by Tan et al. [2]. They conducted galvanostatic copper deposition experiments and showed that, in the absence of chloride ion, either SPS or MPS added to the plating solution inhibited copper deposition. Upon the addition of Cl^-, a transition from inhibition to acceleration was observed for both additives. They also found that the effectiveness of SPS is more dependent on potential than that of MPS, an observation that would suggest a role for faradaic reduction of SPS to MPS.

In the presence of cuprous chloride, both SPS and MPS appear to form complexes with Cu(I), and it has been proposed by a number of investigators that one of these complexes is the effective accelerant. Reduction of SPS to MPS is probably a key initial step in the process, and Vereecken et al. presented rotating ring-disk data indicating that this reduction takes place by homogeneous reaction of SPS with Cu(I) rather than by an interfacial faradaic process [1].

$$2\mathrm{Cu(I)} + \mathrm{SPS} + 2\mathrm{H}^+ = 2\mathrm{Cu(II)} + 2\mathrm{MPS} \tag{3.2}$$

They point out that in a aerated solution, significant amounts of Cu(I) appear only near the copper metal. As a result, the effective accelerant is formed there and not elsewhere in the plating cell.

The reduction of SPS to MPS can also be driven by the deliberate inclusion of another reducing agent in place of Cu(I). So, for example, Volov and West showed that the ferrous/ferric couple can reduce SPS to MPS and hence increase accelerant efficiency [2].

$$2\mathrm{Fe(II)} + \mathrm{SPS} + 2\mathrm{H}^+ = 2\mathrm{Fe(III)} + 2\mathrm{MPS} \tag{3.3}$$

A number of investigators have presented evidence for formation of Cu(I) thiolates by reaction of copper ions with SPS or MPS. Healy et al. found that SPS forms a Cu(I) thiolate and that Cu(II) and MPS react to form a Cu(I) thiolate [3]. They suggested the mechanism

$$4\mathrm{Cu(I)} + \mathrm{SPS} = 2\mathrm{Cu(II)} + 2\mathrm{Cu(I)thiolate} \tag{3.4}$$

Survila et al. proposed the mechanism,

$$2\mathrm{Cu(II)} + 4\mathrm{MPS} = 2\mathrm{Cu(I)thiolate} + \mathrm{SPS} + 4\mathrm{H}^+ \tag{3.5}$$

and they determined an equilibrium K_1 of $10^{3.3}$ for this reaction [4]. Frank and Bard observed a Cu(I)-MPS thiolate by UV–visible spectroscopy and electron paramagnetic resonance spectroscopy [5]. Pasquale et al. reported reaction of Cu(II) with MPS to produce a Cu(I) thiolate product that they confirmed by UV–visible spectroscopy [6]. Okubo, Watanabe, and Kondo, based on rotating ring-disk electrode experiments, suggested formation of two distinct Cu(I)-additive complexes, one from MPS (CuCl-thiolate), the other from SPS [7]. Chen et al., based on electrochemical impedance spectroscopy and linear sweep voltammetry experiments, proposed the formation of a CuCl-MPS complex [8]. Garcia-Cardona et al. used NMR to study reactions of SPS and MPS with Cu(I) and Cu(II) chlorides [9]. In addition to Reaction (3.5), they considered two additional reactions.

$$4\mathrm{Cu(I)} + \mathrm{SPS} = 2\mathrm{Cu(II)} + 2\mathrm{Cu(I)thiolate} \tag{3.6}$$

$$\mathrm{Cu(I)} + \mathrm{nMPS} = [\mathrm{Cu(I)thiolate}_n]^{(n-1)} + \mathrm{nH}^+ \tag{3.7}$$

They found that SPS reacts directly with CuCl to give a Cu(I) thiolate product and Cu(II) with an equilibrium constant K_2 of 5.2×10^{-3} M^{-1}. No evidence for formation of a Cu(I)-SPS or CuCl-SPS complex was found.

Thiolates are not the only products reported in interactions of SPS and copper species. Frank and Bard reported a SPS-Cu(I) complex which retained the disulfide bond, suggesting a sulfonate complex [5]. Schultz and coworkers also proposed formation of a CuCl-SPS complex with sulfonate coordination based on vibrational spectroscopic as well as mass spectral data and density functional theory calculations (see Fig. 3.2) [10]. Tan et al. hypothesized that a MPS thiol acts as an inhibitor while the accelerant effect is due to the MPS sulfonate group [11].

The accelerant function of SPS is known to be affected by aging of the plating solution. Aging may have both positive and negative effects on the accelerant. In commercial plating of interconnects onto wafers, for instance, plating baths may be preconditioned by deposition onto dummy wafers. Depletion of accelerant in plating operations is often a significant factor and may be particularly rapid in pulse-reverse deposition or in the presence of partially submerged anodes. Pulse-reverse plating may completely exhaust the plating bath after just one wafer. At the

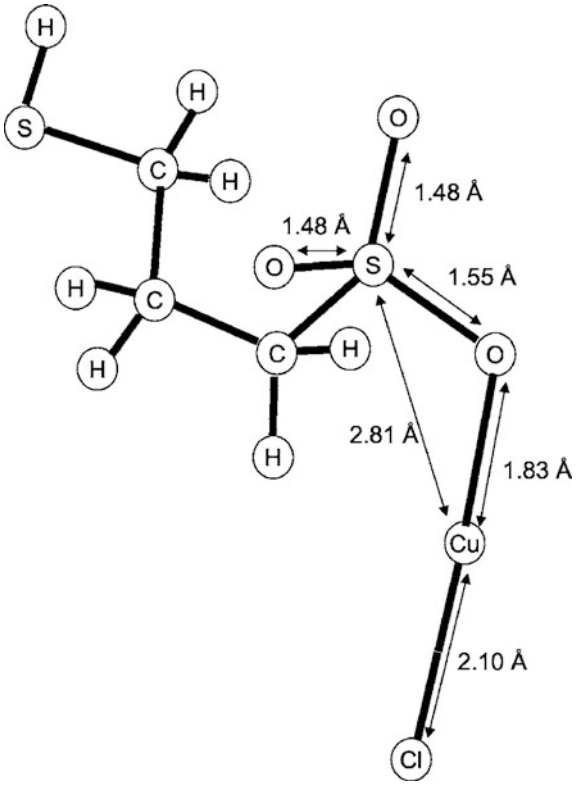

Fig. 3.2 Sulfonate-CuCl complex structure proposed by Schulz et al. Reproduced with permission from Schulz et al. [10]

same time, some transformation of the accelerant additive is essential. Hence, the consumption of accelerant may be integral to its operation or it may result from extraneous processes that could be eliminated through careful design.

A possible pathway for decomposition of SPS to propane disulfonic acid (PDS) is oxidation at the disulfide S–S bond by molecular oxygen or reactive oxygen species.

$$\begin{aligned} &HO_3S\text{--}C_3H_6\text{--}S\text{--}S\text{--}C_3H_6\text{--}SO_3H + 0.5\ O_2 \\ &\quad = > HO_3S\text{--}C_3H_6\text{--}SO\text{--}S\text{--}C_3H_6\text{--}SO_3H \end{aligned} \tag{3.8}$$

$$\begin{aligned} &HO_3S\text{--}C_3H_6\text{--}SO\text{--}S\text{--}C_3H_6\text{--}SO_3H + 0.5\ O_2 \\ &\quad = > HO_3S\text{--}C_3H_6\text{--}SO_2\text{--}S\text{--}C_3H_6\text{--}SO_3H \end{aligned} \tag{3.9}$$

$$\begin{aligned} &HO_3S\text{--}C_3H_6\text{--}SO_2\text{--}S\text{--}C_3H_6\text{--}SO_3H + O_2 \\ &\quad = > H\text{--}C_3H_6\text{--}SO_2\text{--}SO_2\text{--}C_3H_6\text{--}SO_3H \end{aligned} \tag{3.10}$$

$$\begin{aligned} &HO_3S\text{--}C_3H_6\text{--}SO_2\text{--}SO_2\text{--}C_3H_6\text{--}SO_3H + 0.5\ O_2 + H_2O \\ &\quad = > 4HO_3S\text{--}C_3H_6\text{--}SO_3H \end{aligned} \tag{3.11}$$

A heterogeneous faradaic process can also be considered.

$$HO_3S\text{--}C_3H_6\text{--}S\text{--}S\text{--}C_3H_6\text{--}SO_3H + 2H_2O = > HO_3S\text{--}C_3H_6\text{--}SO_2\text{--}S\text{--}C_3H_6\text{--}SO_3H + 4H^+ + 4e^- \quad (3.12)$$

$$HO_3S\text{--}C_3H_6\text{--}SO_2\text{--}S\text{--}C_3H_6\text{--}SO_3H + 4H_2O = > 2HO_3S\text{--}C_3H_6\text{--}SO_3H + 6H^+ + 6e^- \quad (3.13)$$

Hung et al. investigated the products of SPS oxidation in plating solutions by mass spectroscopy [12]. They observed that PDS was the main product of SPS decomposition. Using ion chromatography and electrospray ionization mass spectroscopy, Brennan et al. found that PDS is the most prevalent impurity in commercial SPS and that it is a product of the oxidation of SPS [13]. However, they observed that SPS is stable in air-saturated solution except in the presence of Cu(I). This result is consistent with the fact that Cu(I) is a good catalyst for generation of reactive oxygen species in solution. Gabrielli et al. investigated the influence of soluble and insoluble anodes on accelerant performance. They found that degradation of SPS is more rapid at insoluble anodes due to their higher surface overpotential [14]. Lee et al. also examined the effects of current density and anodic processes of the decomposition of SPS to PDS in plating solutions [15].

3.3 Surface Processes

The presumed mechanism by which the accelerant reactivates a surface that has been inhibited by a suppressor is through removal of the suppressor from the surface either by displacement (competitive adsorption) or by disruption of the suppressor-surface bond. Hence, the affinity of SPS, MPS, or their complexes for adsorption onto the copper surface is central to an understanding of the accelerant mechanism. Tan et al. studied the PEG/Cl^-/SPS system by transient electrochemical methods including voltammetry and accelerant injection [11, 16]. They concluded that the filling effect depends on both a competitive adsorption mechanism as well as consumption of accelerant on the surface. They also found that the presence of chloride is required for strong adsorption of the accelerant. Basol and West used a plating cell equipped with sweeping pad to demonstrate inhibition by adsorbed inhibitor followed by reactivation by the accelerant [17]. Each sweep disproportionately removed the accelerant while leaving a relatively large amount of suppressor on the surface. Within a characteristic time, the accelerant re-adsorbed and restored a higher deposition rate. Bozzini et al. found evidence by Raman spectroscopy for adsorption of SPS in the presence of chloride [18]. Walker et al. found evidence of MPS and SPS adsorption by spectroscopic ellipsometry [19]. Both Taubert et al. [20] and Tu et al. [21] observed similar adsorption by STM. Pasquale reported an adsorbed SPS-Cu species by Raman and IR spectroscopy [6]. Kinetics of suppressor displacement were measured for

several suppressors by Willey and West with a microfluidic cell [22]. By contrast Bae and Gewirth, using cyclic voltammetry, capacitance, and electrochemical scanning tunneling microscopy, concluded that neither SPS nor MPS was strongly adsorbed even in the presence of chloride [23].Walker et al. found that at lower negative overpotential, adsorption of MPS is slower and less potential-dependent than is adsorption of SPS [24]. At higher overpotential the adsorption rate of SPS is more comparable to that of MPS and this is reflected in the potential dependence of the SPS accelerant effect.

Broekmann's group has proposed a detailed mechanism of accelerant action that entails adsorption and dissociation of SPS to MPS followed by deactivation of the suppressor. [25–27] Their data indicate that suppression is due to formation of a branched polymeric complex with Cu(I) on top of a halide adlayer (see Fig. 3.3). This complex is broken up and dissolved by MPS which competes with the complex for Cu(I). Under this hypothesis, the accelerant is generated on the surface, and its generation is promoted by the copper deposition reaction. MPS accumulates on the surface and prevents the formation of the suppressor complex through rupture of the surface-suppressor coordination bond. At the same time, free MPS in the near surface solution may dissolve the suppressor complex through competition for Cu(I). This latter mechanism involves a free MPS accelerant that is not adsorbed.

3.4 Filling Mechanism

The literature presents two types of models to account for filling by suppressor-accelerant additive ensembles. The first is based on concentration of surface-confined accelerant by elimination of surface area during growth in recesses (see Fig. 3.4) [28, 29]. This model was developed to simulate filling of submicron features on short time scales. The second type of model is based on a favorable distribution of suppressor and accelerant within a feature that is a result of both mass transfer and competitive adsorption. It was developed to account for filling of larger features, such as through-silicon vias (TSV) over much longer periods of time (see Fig. 3.5) [30–33]. This latter type may incorporate features of both mechanisms [33]. However, bottom-up filling in features of this scale has been demonstrated in the absence of curvature [34, 35]. In addition, some attention has been given to the effect of a transport-limited oxidizer [36, 37].

Moffat et al. introduced a model based on local accumulation of accelerant on the surface [28]. The increase in local surface concentration is due to the decrease in surface area during growth on a concave surface. This model provides a mechanism for bottom-up fill in submicrometer trenches (see Fig. 3.6). In an initially square trench, the points of highest curvature, and hence most rapid acceleration in growth rate, are the bottom corners. As these fill in, the maximum curvature shifts toward the bottom of the trench. Hence, after a short time, the highest deposition rate prevails at the bottom, resulting in bottom-up fill.

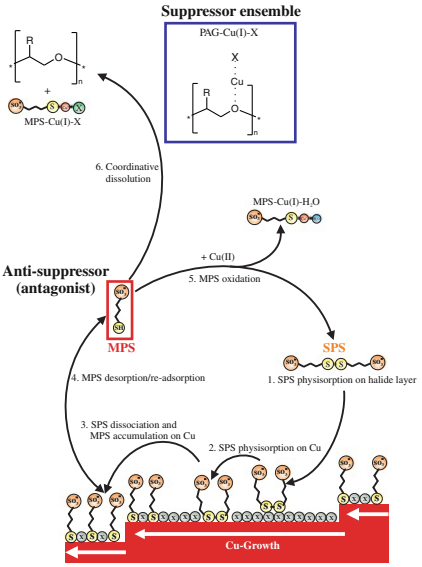

Fig. 3.3 Displacement of suppressor by accelerant. Reproduced with permission from Huynh et al. [27], their Fig. 3.1

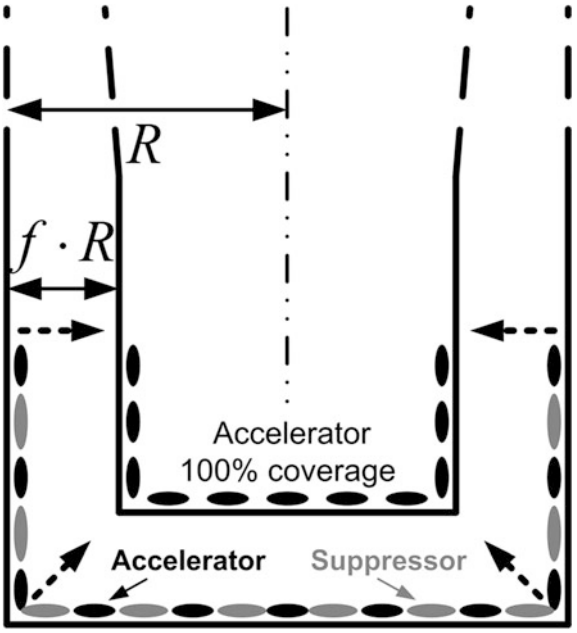

Fig. 3.4 Schematic of superfilling mechanism based on the surface-contraction model. Reproduced with permission from Adolf and Landau [33] (their Fig. 3.2)

The mechanism also accounts for the lag between the beginning of deposition and the onset of bottom-up fill, since the accelerant is only concentrated at points of high curvature after some shape change has occurred. Finally, it accounts for the overburden or bump above the filled trench. Bump formation is driven by the fact

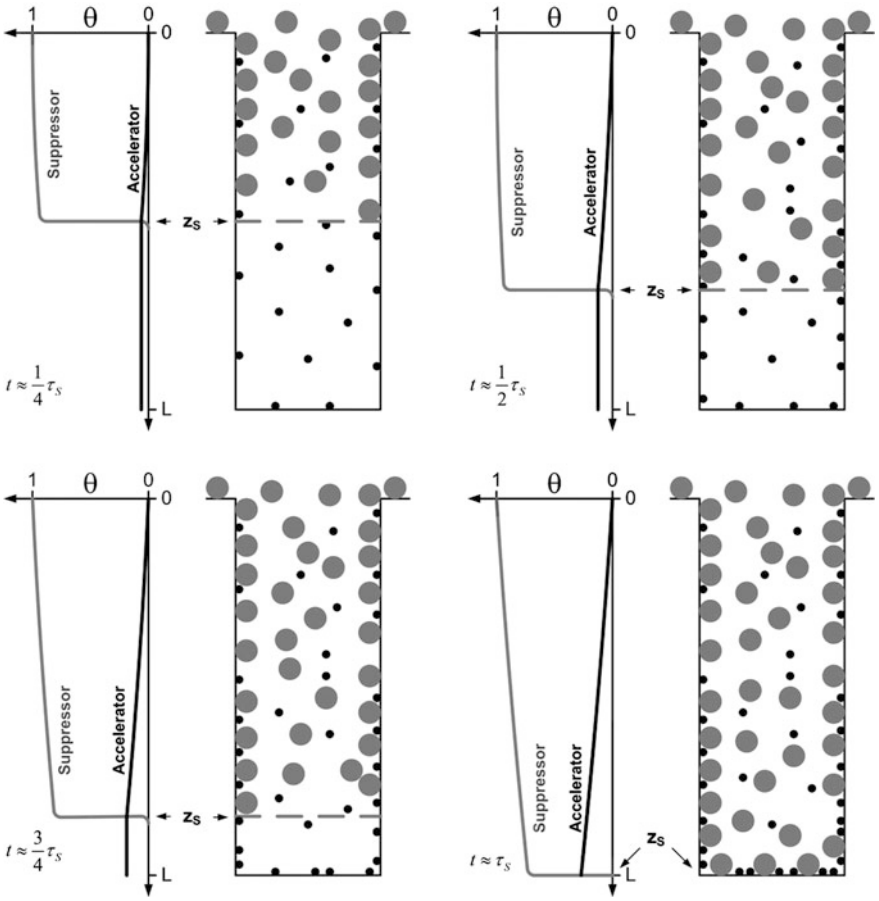

Fig. 3.5 Schematic of superfilling based on the transport model. Reproduced with permission from Adolf and Landau [33] (their Fig. 3.1)

that the high concentration of accelerant at the bottom of the feature carries over to the wafer plane after the feature is filled.

West, Mayer, and Reid independently formulated a similar model at the same time [29]. They also emphasized that the model provides a mechanism for bottom-up fill and accounts for bump formation after feature filling. Their discussion addresses the fact that this type of model introduces dynamic surface phenomena into leveling models that had previously considered only bulk transport. Both groups showed that hysteretic cyclic voltammetry curves, in which the current on a return sweep is higher than current on a cathodic sweep, is a characteristic of super filling plating baths (see Fig. 3.7). This hysteresis is the result of reactivation of the suppressed surface by adsorbed accelerant.

Akolkar and Landau presented a suppressor-accelerant model that emphasizes time-dependent transport of additives coupled with adsorption in filling of larger

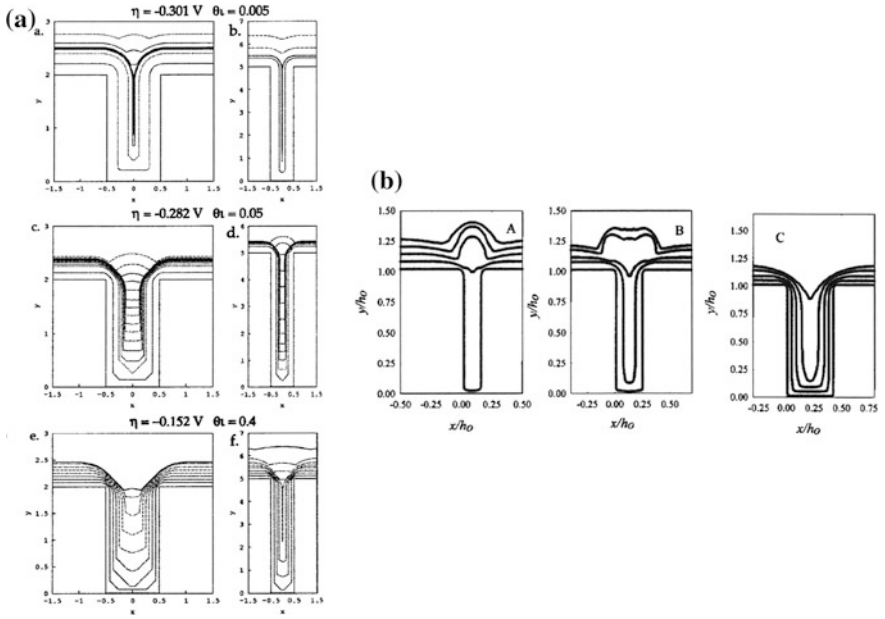

Fig. 3.6 Simulations of trench filling by the surface-contraction model. **a** Reproduced with permission from Moffat et al. [28], their Fig. 3.2 and **b** Reproduced with permission from West et al. [29], their Fig. 3.1

scale features such as through-silicon vias (see Fig. 3.5) [31, 32]. This model includes the instantaneous initial depletion of suppressor within the via by kinetically fast adsorption on the side walls and bottom, followed by diffusion of suppressor from the via exterior to the via bottom. The slow transport of suppressor is due to both its relative low diffusivity compared with the accelerant and to the fact that its transport down the via is hindered by adsorption on the via sidewalls. Adsorption of the accelerant by contrast is not transport limited. Rather its rate is controlled by adsorption kinetics. Bottom-up filling is thus promoted by two distinct competitions between suppressor and accelerant. The first is adsorption of accelerant near the via bottom where the suppressor concentration is low, preventing suppressor adsorption. The second is adsorptive displacement of suppressor by accelerant further up the via at longer times. Each of these steps is characterized by a time constant. The mechanism is effective in high aspect ratio vias where the initial depletion of suppressor is rapid.

Transient bulk-diffusion phenomena are most important in filling of large features because the dimensions of these features produce sufficiently long diffusion times. In filling of submicrometer features, bulk diffusion reaches a steady state before the onset of bottom-up filling. The transport-diffusion model on larger scales does not require curvature to predict bottom-up fill. This fact has been demonstrated experimentally by Kondo and coworkers deposition into holes in

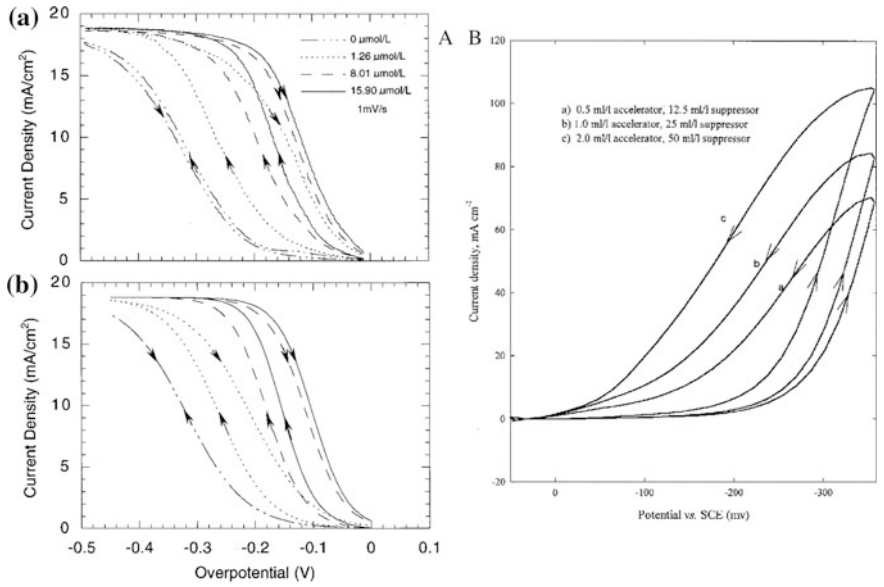

Fig. 3.7 Hysteresis loop **a** Reproduced with permission from Moffat et al. [28], their Fig. 3.2 and **b** Reproduced with permission from West et al. [29], their Fig. 3.1

insulating masks on copper foil [34, 35]. In this configuration, the problem is nearly one dimensional, and the growing surface remains flat throughout. Yet, thicker masks result in more rapid growth. The result can be understood by application of the transport-adsorption mechanism, although it differs in some detail due to the absence of side walls, and the more rapid diffusion of accelerant compared with that of suppressor is consistent with the experimental observation in these experiments. (see Fig. 3.8). As in TSV filling, the suppressor is adsorbed at a rate controlled by diffusion to the via bottom. The accelerant wins the race to the via bottom because of its higher diffusion constant and eventually displaces the suppressor altogether.

The effects of competitive diffusion phenomena, where the accelerant arrives more rapidly at a feature bottom than does the suppressor, can be amplified by addition of oxidizers to the bulk solution (see Fig. 3.8). Examples include ozone [36] and oxygen [37]. Because formation of the effective accelerant proceeds through reduction of SPS to MPS by Cu(I), an oxidizing environment can inhibit accelerant production either by oxidation of MPS or oxidation of Cu(I). In this instance, it is the diffusion limitation on the oxidizer that promotes filling. The oxidizer deactivates the accelerant near the tops of features. Because it is consumed in the process, it does not penetrate deeply into the via and cannot deactivate the accelerant near the bottom of features. This effect appears to connect the various filling models with the accelerant chemistry because the oxidizers act by destruction of the Cu(I)thiolate.

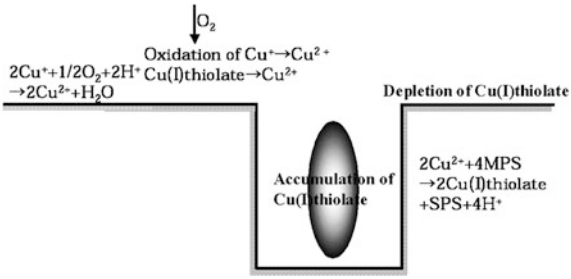

Fig. 3.8 Schematic of super filling based on the free accelerant model with oxidative destruction of accelerant. Reproduced with permission from Kondo et al. [35]

The formation of cuprous is a crucial intermediate and the cuprous intermediate is always produced during the electrodepositon process.

$$Cu^{2+} + e^- \underset{k_{-1}}{\overset{k_1}{\rightleftarrows}} Cu^+ \tag{3.14}$$

$$Cu^{2+} + e^- \underset{k_{-1}}{\overset{k_2}{\rightleftarrows}} Cu^+ \tag{3.15}$$

These reactions are reversible processes. The reaction constant k_1 for the cupric ions to cuprous ions is $2x10^{-4}$ mol·m^{-2}s^{-1}and k_{-1} for the cuprous to cupric ions is 8×10^{-3} mol·m^{-2}s^{-1}. k_2 for the cuprous ions to metallic copper is 130 mol·m^{-2}s^{-1} and k_{-2} for the metallic copper to cuprous ions is $3.9x10^{-7}$ mol·m^{-2}s^{-1}. Large value of k_2 for 130 mol.m^{-2}s^{-1} means that once the cuprous ions is formed, the reaction to reduce it to metallic copper is extremely rapid [38]. Furthermore, the cuprous ions are transparent and odorless. Hence it is extremely difficult to detect the cuprous ions and accordingly few studies exist which are related to the acceleration effect of cuprous ions.

On the other hand, a rotating ring disk electrode (RRDE) has been used to detect the cuprous ions. The cuprous ions detected at the ring of the RRDE is 1,000 times higher for the copper dissolution, if it is compared to the cuprous ions for the electrodeposition [39]. Hence, we formed a large amount of cuprous ions within the confined area of the trench in the trench bottom electrodes and experimentally verify the relation between the cuprous ions and acceleration. The trench bottom electrodes have been photo-lithographed on the copper foil with OFPR-800-(Tokyo-oka) photoresist. The trench widths are 3, 5, and 10 μm.

This work is from Kondo and coworker's recent researches [40, 41]. The effect of the O_2 bubbling and N_2 bubbling has been initially tested in the nonstirred bath. The bath consists of the basic bath and 1ppm SPS, 400 ppm PEG and 50 ppm Cl^-. Prior to the LSVs, the cuprous ions were formed by dissolving the copper electrode at the trench bottom for 12s at 10 mA/cm^2. Figure 3.9a shows the LSV result with N_2 bubbling. The potential and current density are illustrated for the trench bottom electrode widths of 3, 5, and 10 μms. Drastic increases in the current densities due to the acceleration effect are observed and the current density increased up to

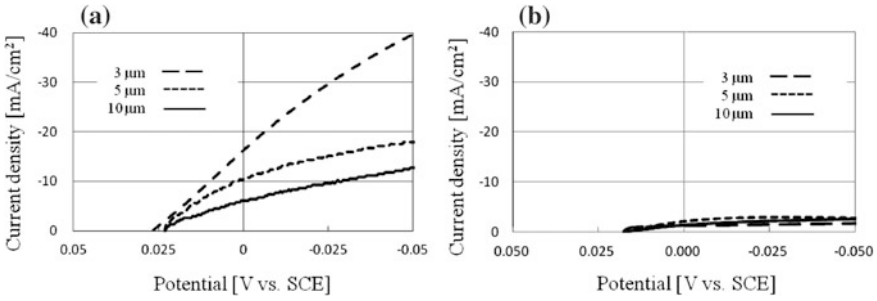

Fig. 3.9 **a** Result of LSV measurements with N_2 bubbling. **b** Result of LSV measurements with O_2 bubbling. SPS:1 ppm, Cl^-:50 ppm, PEG:400 ppm

-40 mA/cm^2 for the 3 μm trench bottom electrode width at -0.05V vs. SCE. Furthermore, the current densities increase with the narrower trench bottom electrode width. On the contrary, the currents show a very low value of -1.0mA/cm^2 for the LSV result with O_2 bubbling Fig. 3.9b. The current densities are same with the trench bottom electrode widths of 3, 5, and 10 μms. The drastic difference in the current densities with the O_2 gas concentration in the electrolyte must be caused by the cuprous complex formed in the trench of the trench bottom electrode. The increase in the current densities for the narrower trench of the trench bottom electrode must be caused by the accumulation of a cuprous complex in the trench.

In order to prove that this cuprous complex is free, floating in the electrolyte, and not adsorbing on the electrode, forced convection has been applied by the stirrer at 600 rpm. The current densities have been then measured by LSV by initially dissolving the copper electrode at the trench bottom. The LSV measurements are shown in Fig. 3.10a. The current densities decrease to a few mA/cm^2 and almost no difference in the current densities for the trench widths of 3, 5, and 10 μm. The acceleration effect has deceased. This is because the free cuprous complex flows out of the trenches due to the stirring at 600 rpm.

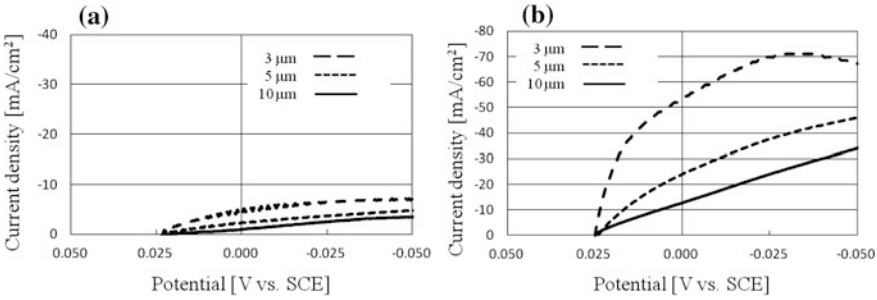

Fig. 3.10 **a** Result of LSV measurements with N_2.Stirring rate of stirrer is 600 rpm. SPS:1 ppm, Cl^-:50 ppm, PEG:400 ppm.**b** Result of LSV measurements with N_2 bubbling. Cl^-:50 ppm

Next, in order to investigate the cuprous ions and the additives, we have eliminated the additives and the LSVs have been measured. We then have eliminated PEG and SPS and only the Cl^- has added. The current shows a marked increase for $-70mA/cm^2$ for 3 μm at $-0.05V$ vs. SCE Fig. 3.10b. The narrower the trench is the current densities increase. Cl^- is an important additive for the acceleration, and the acceleration must be related to the free cuprous complex and electron bridge formation of Cl^- [42], which may be enlarging reaction constant of k_1 in eq. (1) through the electron bridge formation.

Without dissolving copper at the trench bottom electrodes, the current densities have been measured at the constant potential of $-0.15V$ vs. SCE. This is because we want to prove that the cuprous forming through the electrodeposition process is an accelerator. With O_2 bubbling, the current densities are low values of about 1.0 mA/cm^2. However, the current densities markedly increase with the N_2 bubbling. With the narrower trenches, the current densities increase and $-23mA/cm^2$ has been measured for the 3 μm trench width. These constant potential measurements without dissolving the copper electrode also show that the free cuprous complex formed through electrodeposition is the accelerant.

3.5 Summary

Investigations over the last two decades have produced considerable insight into the nature and mechanism of copper-plating accelerants. Nevertheless, there remain disagreements and uncertainties over the configuration of the accelerant and its mechanism of action. It appears that there are substantial constraints on the molecular structure of accelerants, and as a result suitable molecules are few. This review has focused on SPS/MPS. The mechanism of action of the accelerant SPS/MPS is complicated in comparison to that of suppressors and levelers. It involves reversible transformations of the additive through interactions with at least two other species in solution and with the metal. Chloride is essential to formation of the accelerant complex. In addition, Cu(I) must be present or be formed at the metal-solution interface as well. The transformations among SPS, MPS, and accelerant complex are probably reversible and may run through a cycle. In addition, there are irreversible transformations that may take place in the presence of oxidizers or at the anode, and these can result in rapid consumption of the accelerant in practical operations.

The most widely held view is that SPS/MPS forms a Cu(I) thiolate that deactivates suppressors such as PEG, although it is not settled whether the complex is formed in solution or on the metal surface. Deactivation of the suppressor may proceed by competitive adsorption and displacement or by disruption of the suppressor-surface bond either by a free accelerant or an adsorbed accelerant. It is possible that either mechanism may be important depending on the character of the suppressor, and the literature demonstrates that the interaction between suppressor and accelerant is complicated, involving complexes of both components with

Cu(I) and Cl^-. The mechanism by which suppressor-accelerant combinations produce filling is complicated as well. The role of accelerants in filling may be controlled by surface processes or by bulk-diffusion processes depending on the feature scale and filling time. Their effectiveness may also be enhanced by the use of reducing agents.

This review has highlighted a relatively small part of the literature. The number of publications on the topic is large. More attention has been paid to solution chemistry and to accelerant-suppressor interactions and less to the very large literature on super filling. These topics are addressed in detail elsewhere in this volume.

Acknowledgments The author acknowledges many helpful suggestions provided by Professor Edward H. Wong.

References

1. Vereecken PM, Binstead RA, Deligianni H, Andricacos PC (2005) The chemistry of additives in copper Damascene plating. IBM J Res Dev 49:3–19
2. Tan M, Guymon C, Wheeler DR, Harb JN (2007) The role of SPS, MPSA, and chloride in additive systems for copper electrodeposition. J Electrochem Soc 154:D78–D81
3. Healy JP, Pletcher D (1992) The chemistry of additives in an acid copper electroplating bath. J Electroanal Chem 338:167–177
4. Survila A, Kanapeckaite S, Pauliukaite R (1998) Polaragraphic behavior of Cu(II) solutions involving 3-Mercapto-1-Propanosulphonic Acid. Chemija 1:21–26
5. Frank A, Bard AJ (2003) The decomposition of the sulfonate additive sulfopropyl sulfonate in acid copper electroplating chemistries. J Electrochem Soc 150:C244–C250
6. Pasquale MA, Bolzan AE, Guida JA, Piatti RCV, Arvia AJ, Piro OE, Castellano EE (2007) A new polymeric [Cu(SO3(CH2)3SeS(CH2)3SO3)(H2O)4]n complex molecule produced from constituents of a super-conformational copper plating bath: Crystal structure, infrared and Raman spectra and thermal behavior. Solid State Sci 9:862–868
7. Okubu T, Watanabe K, Kondo K (2007) Analytical study of the characteristics of Cu(I) species for the via-filling electroplating using a RRDE. J Electrochem Soc 154:C181–C187
8. Chen H-M, Parulekar SJ, Zdunek A (2008) Interactions of chloride and 3-Mercapto-1-Propane sulfonic acid in acidic copper sulfate electrolyte. J Electrochem Soc 155:D349–D356
9. Garcia-Cardona E, Wong EH, Barkey DP (2011) NMR spectral studies of interactions between the accelerants SPS and MPS and copper chlorides. J Electrochem Soc 158:D143–D148
10. Schultz ZD, Feng ZV, Biggin ME, Gewirth AA (2006) Vibrational spectroscopic and mass spectrometric studies of the interaction of Bis(3-sulfopropyl)-disulfide with Cu surfaces. J Electrochem Soc 153:C97–C107
11. Volov I, West AC (2011) Interaction between SPS and MPS in the presence of ferrous and ferric ions. J Electrochem Soc 158:D456–D461
12. Hung C-C, Lee W-H, Hu S-Y, Chang S-C, Chen K-W, Wang Y-L (2008) Investigation of Bis-(3-sodiumsulfopropyl disulfide) (SPS) decomposition in a copper-electroplating bath using mass spectroscopy. J Electrochem Soc 155:H329–H333
13. Brennan, RG, Philips, MM, Ou Yang, L-Y, Moffat, TP (2011) Characterization and purification of commercial SPS and MPS by ion chromatography and mass spectrometry. J Electrochem Soc 158:D178–D186

14. Gabrielli C, Mocoteguy P, Perrot H, Zdunek A, Nieto-Sanz D (2007) Influence of the anode on the degradation of the additives in the Damascene process for copper deposition. J Electrochem Soc 154:D163–D169
15. Lee W-H, Hung C-C, Chang S-C, Wang Y-L (2010) Bis-(3-sodiumsulfopropyl disulfide) decomposition with cathodic current flowing in a copper-electroplating bath. J Electrochem Soc 157:H131–H135
16. Tan M, Harb JN (2003) Additive behavior during copper electrodeposition in solutions containing Cl^-, PEG, and SPS. J Electrochem Soc 150:C420–C425
17. Başol BM, West AC (2006) Study on mechanically induced current suppression and super filling mechanisms. Electrochem Solid-State Lett 9:C77–C80
18. Bozzini B, D'Urzo L, Romanello V, Mele C (2006) Electrodeposition of Cu from acidic sulfate solutions in the presence of Bis-(3-sulfopropyl)-disulfide (SPS) and chloride ions. J Electrochem Soc 153:C254–C257
19. Walker ML, Richter LJ, Moffat TP (2006) Competitive adsorption of PEG, Cl^-, and SPS/MPS on Cu: an in situ ellipsometric study. J Electrochem Soc 153:C557–C561
20. Täubert CE, Kolb DM, Memmert U, Meyer H (2007) Adsorption of the additives MPA, MPSA, and SPS onto Cu(111) from sulfuric acid solutions. J Electrochem Soc 154:D293–D299
21. Tu H-L, Yen P-Y, Chen S, Yau S-L, Dow W-P, Lee Y-L (2011) In situ imaging of Bis-3-sodiumsulfopropyl-disulfide molecules adsorbed on copper film electrodeposited on Pt(111) single crystal electrode. Langmuir 27:6801–6807
22. Willey MJ, West AC (2007) SPS adsorption and desorption during copper electrodeposition and its impact on PEG adsorption. J Electrochem Soc 154:D156–D162
23. Bae S-E, Gewirth AA (2006) In situ EC-STM studies of MPS, SPS, and chloride on Cu(100): structural studies of accelerators for dual Damascene electrodeposition. Langmuir 22:10315–10321
24. Walker ML, Richter LJ, Moffat TP (2007) Potential dependence of competitive adsorption of PEG, Ci- and SPS/MPS on Cu: an in situ ellipsometric study. J Electrochem Soc 154:D277–D282
25. Hai NTM, Kramer KW, Fluegel A, Arnold M, Mayer D, Broekmann P (2012) Beyond interfacial anion/cation pairing: the role of Cu(I) coordination chemistry in additive-controlled copper plating. Electrochim Acta 83:367–375
26. Hai NTM, Huynh TMT, Fluegel A, Arnold M, Mayer D, Reckien W, Broekmann P (2012) Competitive anion/anion interactions on copper surfaces relevant for Damascene electroplating. Electrochim Acta 70:286–295
27. Huynh TMT, Weiss F, Hai NTM, Reckien W, Bredow T, Fluegel A, Arnold M, Mayer D, Keller H, Broekmann P (2013) On the role of halides and thiols in additive-assisted copper electroplating. Electrochim Acta 89:537–548
28. Moffat TP, Wheeler D, Huber WH, Jossell D (2001) Superconformal electrodeposition of copper. Electrochem Solid-State Lett 4:C26
29. West AC, Mayer S, Reid J (2001) A superfilling model that predicts bump formation. Electrochem Solid-State Lett 2001(4):C50–C53
30. Chalupa R, Cao Y, West AC (2002) Unsteady diffusion effects on electrodeposition into a submicron trench. J Appl Electrochem 32:135–143
31. Akolkar R, Landau U (2004) A time-dependent transport-kinetics model for additive interactions in copper interconnect metallization. J Electrochem Soc 151:C702–C711
32. Akolkar R, Landau U (2009) Mechanistic analysis of the 'bottom-up' fill in copper interconnect metallization. J Electrochem Soc 156:D351–D359
33. Adolf J, Landau U (2011) Predictive analytical fill model of interconnect metallization providing optimal additives concentrations. J Electrochem Soc 158:D469–D476
34. Kondo K, Yamakawa N, Tanaka Z, Hayashi K (2003) Copper Damascene electrodeposition and additives. J. Electroanalytical Chem. 559:137–142

35. Kondo K, Matsumoto T, Watanabe K (2004) Experimental study on inhibition and acceleration effects role of additives for copper Damascene electrodeposition. J Electrochem Soc 151:C250–C255
36. Mazur S, Jackson CE Jr (2008) Enhanced electrodeposition of Cu into recessed features via topographically selective ozonolysis of adsorbed accelerator. J Electrochem Soc 155:D608–D613
37. Kondo K, Yonezawa T, Mikami D, Okubo T, Taguchi Y, Takahashi K, Barkey DP (2005) High-aspect-ratio copper-via-filling for three-dimensional chip stacking; II. reduced electrodeposition process. J Electrochem Soc 152:H173–H177
38. Tantavishet N, Pritzker M (2003) Low- and high-frequency pulse current and pulse reverse plating of copper. J Electrochem Soc 150:C665–C670
39. White JR (1987) Reverse pulse plating of copper from acid electrolyte; a rotating ring disk electrode study. J Applied Electrochem 17:977–982
40. Kondo K, Hamazaki K, Yokoi M, Okamoto N, Saito T (2013, in present) Behavior of cuprous intermediate in copper damascene electrodeposition. ECS Electrochem. Lett.,In course of publication
41. Kondo K, Hamazaki K, Yokoi M, Okamoto N, Saito T (2013, in present) Behavior of cuprous intermediate in copper damascene electrodeposition. ECS 2013 Fall Meeting in SanFransisco, Abstract 2086
42. Nagy Z, Blaudeau JP, Hung NC, Curtiss LA, Zurawski DJ (1995) Chloride ion catalysis of the copper deposition reaction. J.Electrochem Soc 142:L87–L92